

Lock-in transitions in $\text{ErNi}_2\text{B}_2\text{C}$ and $\text{TbNi}_2\text{B}_2\text{C}$

C. Detlefs,^{1,*} C. Song,^{2,†} S. Brown,³ P. Thompson,³ A. Kreyssig,⁴ S. L. Bud'ko,² and P. C. Canfield²

¹European Synchrotron Radiation Facility, Boîte Postale 220, 38043 Grenoble Cedex, France

²Ames Laboratory and Department of Physics and Astronomy, Iowa State University, Ames, IA 50011

³XMAS CRG, European Synchrotron Radiation Facility,

Boîte Postale 220, 38043 Grenoble Cedex, France

⁴Institut für Angewandte Physik (IAPD), Technische Universität Dresden, 01062 Dresden, Germany

(Dated: Version May 25, 2020)

High resolution x-ray magnetic scattering has been used to determine the variation with temperature of the magnetic modulation vector, τ , in $\text{ErNi}_2\text{B}_2\text{C}$ and $\text{TbNi}_2\text{B}_2\text{C}$ to study the interplay between the weakly ferromagnetic (WFM) phase and proposed lock-in transitions in these materials. At temperatures below the WFM transitions, the modulation wave vectors are within the resolution limit of the commensurate values $11/20$ and $6/11$ for $\text{ErNi}_2\text{B}_2\text{C}$ and $\text{TbNi}_2\text{B}_2\text{C}$, respectively.

PACS numbers: 74.25.Ha, 75.25.+z, 61.10.Eq

Investigations of the physical properties of the superconducting rare-earth nickel boride-carbides, $R\text{Ni}_2\text{B}_2\text{C}$ ($R = \text{Gd-Lu, Y}$), continue to provide insight into the interplay between superconductivity and magnetism (For recent overviews, see refs. 1,2.)

Recently, $\text{ErNi}_2\text{B}_2\text{C}$ attracted special attention when the possible coexistence of superconductivity and weak ferromagnetism (WFM) was indicated by several measurements^{3,4,5}. A similar WFM state also exists in $\text{TbNi}_2\text{B}_2\text{C}$ ^{6,7,8}. The similarity of the crystallographic and magnetic properties of these compounds suggests a common origin of the WFM⁹. In order to study the interplay between WFM and the dominant antiferromagnetic (AFM) order we have performed a comparative study of these two compounds using the technique of x-ray resonant magnetic scattering.

In $\text{ErNi}_2\text{B}_2\text{C}$, superconductivity is observed below $T_C = 10.5$ K. Neutron diffraction experiments^{10,11} show that below $T_N = 6.0$ K it orders in a transverse spin density wave with modulation wave vector $\tau_a \approx (0.55, 0, 0)$ and magnetic moments aligned parallel to the $(0, 1, 0)$ -axis of the crystal. As the temperature is lowered, higher harmonic satellites develop, indicating that the spin density wave squares up; the modulation wave vector was reported to be approximately independent of temperature^{10,11}.

A phase transition into a state with a weak ferromagnetic (WFM) component of about $0.33 \mu_B/\text{Er}$ (at $T = 2$ K) is observed at $T_{\text{WFM}} \approx 2.3$ K^{3,4,5}. Whereas this transition is clearly resolved in zero-field specific heat measurements³, the magnetic moment of the ground state has to be extrapolated from magnetization measurements at finite fields above H_{C1} ³. The structure and origin of this WFM state remain unclear. Recently, neutron scattering^{12,13} showed that the WFM state is intimately linked to the appearance of *even* order harmonic components of the spin wave and a lock-in of the modulation wave vector, τ , onto a commensurate position. However, the values of τ these two groups cite do not agree: Whereas Choi et al.¹² find $\tau = 0.548$, Kawano-Furukawa et al.¹³ report $\tau = 11/20 = 0.55$.

Finally, an increase of the scattered intensity at nuclear Bragg peaks confirmed the presence of a WFM component^{4,12}.

Because of the striking similarities in their magnetic properties, it is useful to compare $\text{ErNi}_2\text{B}_2\text{C}$ to $\text{TbNi}_2\text{B}_2\text{C}$. Whereas the latter is not superconducting, it displays the same local moment anisotropy in the paramagnetic phase (easy axes $(1, 0, 0)$ and $(0, 1, 0)$) and forms an AFM structure closely related to that of $\text{ErNi}_2\text{B}_2\text{C}$. In neutron scattering experiments⁷ the magnetic modulation wave vector is found to decrease from $\tau = (0.551, 0, 0)$ at $T_N = 14.9$ K to $(0.545, 0, 0)$ below $T_{\text{WFM}} \approx 7$ K. Unlike in the Er compound, the Tb magnetic moments are aligned *parallel* to the modulation wave vector, forming a *longitudinal* spin wave. Furthermore, a phase transition to a WFM state similar to that of $\text{ErNi}_2\text{B}_2\text{C}$, albeit in the absence of superconductivity, occurs around $T_{\text{WFM}} \approx 7$ K^{6,14}, with magnetic moment $\approx 0.55 \mu_B/\text{Tb}$ at $T = 2$ K. Again, the neutron experiments⁷ indicate that the appearance of a WFM moment may be related to a lock-in of the AFM spin wave to a commensurate propagation vector, in this case $\tau = 6/11 = 0.545$.

A recent Ginzburg-Landau type analysis⁹ shows that a lock-in to $\tau = M/N\mathbf{G}$ (\mathbf{G} = reciprocal lattice vector) with M even and N odd directly induces weak ferromagnetism as secondary order. This result is confirmed by a mean field analysis¹⁵ of $\text{ErNi}_2\text{B}_2\text{C}$.

In both compounds the magnetic ordering transitions are accompanied by structural distortions which lower the crystal symmetry from tetragonal (space group $I4/mmm$) to orthorhombic ($Immm$)^{16,17,18}. This distortion breaks the symmetry between the $(1, 0, 0)$ and $(0, 1, 0)$ crystallographic directions and thus leads to an unique easy axis of the magnetic moment ($\mu \parallel (0, 1, 0)$ in $\text{ErNi}_2\text{B}_2\text{C}$, and $\mu \parallel (1, 0, 0)$ in $\text{TbNi}_2\text{B}_2\text{C}$) and the modulation wave vector ($\tau \parallel (1, 0, 0)$ in both compounds^{19,20}). Since these magneto-elastic effects were not reported in the earlier studies^{7,12,13}, it appears doubtful that they had the resolution necessary to clearly resolve a lock-in transition into a commensurate state. We there-

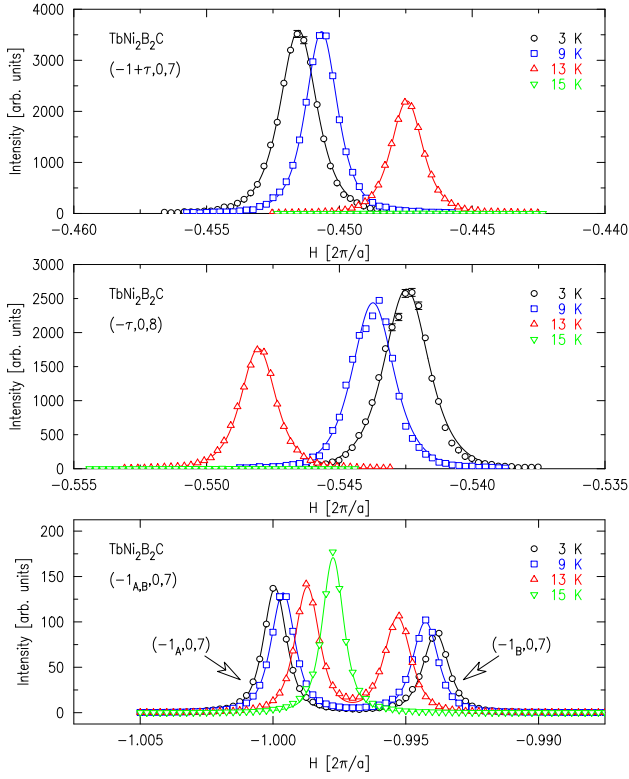


FIG. 1: Scans along the $(H, 0, 0)$ direction of reciprocal space through the $(-1 + \tau, 0, 7)$ (top), $(-\tau, 0, 8)$ (middle), and $(1_{A,B}, 0, 7)$ (bottom) reflections of $\text{TbNi}_2\text{B}_2\text{C}$ at selected temperatures. The horizontal scale is given by the experimental orientation matrix defined at $T = 1.7$ K. Note that the shift in position of the magnetic peaks is comparable to the shift of the structural peak due to the magneto-elastic effects. The width of the magnetic peaks is approximately $1.6 \times 10^{-3} \frac{2\pi}{a}$.

fore performed high-resolution resonant magnetic scattering experiments using synchrotron x-rays^{21,22} on both $\text{ErNi}_2\text{B}_2\text{C}$ and $\text{TbNi}_2\text{B}_2\text{C}$.

Single crystals of $\text{ErNi}_2\text{B}_2\text{C}$ and $\text{TbNi}_2\text{B}_2\text{C}$ were grown at the Ames Laboratory using a high-temperature flux growth technique^{23,24}. Platelets extracted from the flux were examined by x-ray diffraction and were found to be high quality single crystals with the $(0, 0, 1)$ -axis perpendicular to their flat surface. The $\text{ErNi}_2\text{B}_2\text{C}$ sample was cut perpendicular to the $(1, 0, 0)$ direction and the resulting face was mechanically polished to obtain a flat, oriented surface for x-ray diffraction. The sample dimensions after polishing were approximately $2 \times 1.5 \times 0.5$ mm³. The $\text{TbNi}_2\text{B}_2\text{C}$ sample, the same one used in our earlier studies^{17,20}, had a $(0, 0, 1)$ polished face.

The synchrotron experiments were carried out at XMAS CRG and at the Troika undulator beamline (ID10C) of the European Synchrotron Radiation Facility (ESRF). The samples were mounted on the cold finger of a Displex closed cycle refrigerator equipped with an additional Joule-Thompson stage²⁸. The base temperature of this configuration was approximately 1.7 K.

Fig. 1 shows scans through selected magnetic and

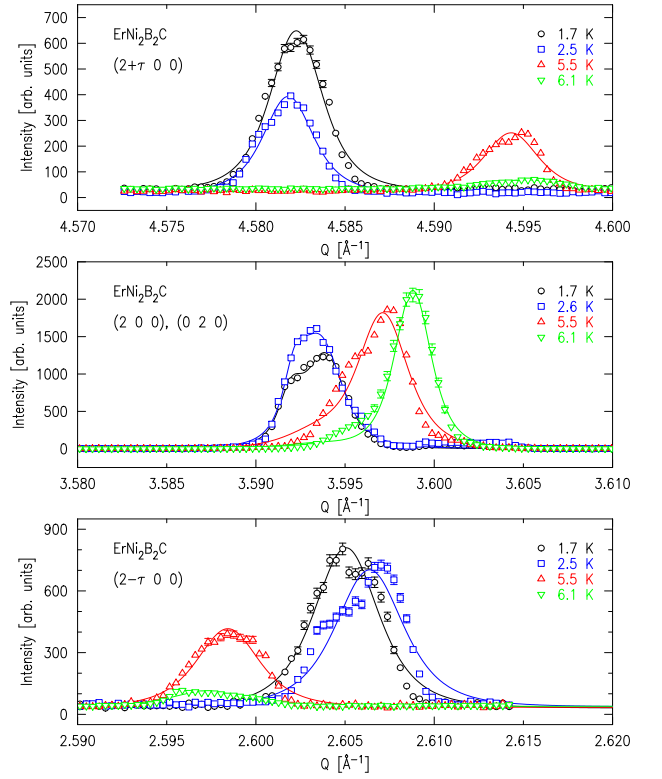


FIG. 2: Longitudinal scans through the $(2 \pm \tau, 0, 0)$ (top, bottom) and $(2, 0, 0)$ (middle) reflections of $\text{ErNi}_2\text{B}_2\text{C}$ at selected temperatures. The width of the peaks is approximately $2.0 \times 10^{-3} \frac{2\pi}{a} = 3.6 \times 10^{-3} \text{ \AA}^{-1}$.

charge reflections of $\text{TbNi}_2\text{B}_2\text{C}$. The variation of the a -axis lattice parameter is significant and has to be taken into account when calculating the modulation wave vector¹⁹ (the horizontal scale is identical in all three panels). The corresponding raw data for $\text{ErNi}_2\text{B}_2\text{C}$ are shown in Fig. 2.

The data presented in Fig. 1 were fitted to a Lorentzian-squared line shape. τ in units of the reciprocal lattice was calculated from

$$\frac{2\pi}{a} = -Q_H(-1 + \tau, 0, 7) - Q_H(-\tau, 0, 8) \quad (1)$$

$$\tau = \frac{Q_H(-\tau, 0, 8)}{Q_H(-1 + \tau, 0, 7) + Q_H(-\tau, 0, 8)}, \quad (2)$$

where $\mathbf{Q} = (Q_H, Q_K, Q_L)$ is the scattering vector. The resulting data are presented in Fig. 3.

For the case of $\text{ErNi}_2\text{B}_2\text{C}$ a similar calculation was applied to the measured positions of the $(2 \pm \tau, 0, 0)$ magnetic Bragg reflections¹⁹:

$$\frac{2\pi}{a} = \frac{1}{2} [Q(2 + \tau, 0, 0) + Q(2 - \tau, 0, 0)] \quad (3)$$

$$\tau = \frac{[Q(2 + \tau, 0, 0) - Q(2 - \tau, 0, 0)]}{[Q(2 + \tau, 0, 0) + Q(2 - \tau, 0, 0)]}. \quad (4)$$

The resulting data are presented in Fig. 4.

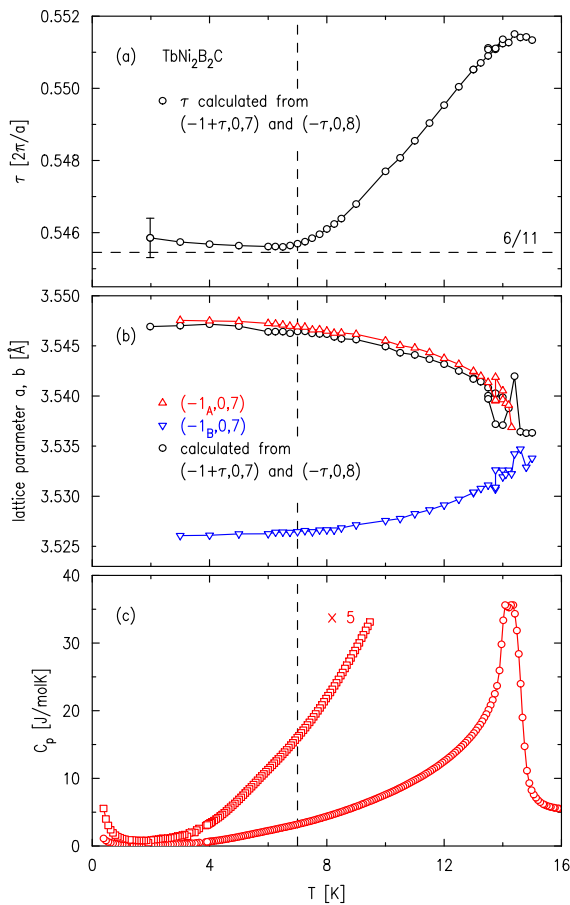


FIG. 3: (a) Around 7 K, the modulation wave vector, τ , of TbNi₂B₂C locks in to the commensurate value of 6/11, indicated by the dashed line. (b) Basal plane lattice parameters, a and b , extracted from the position of the $(-1_{A,B}, 0, 7)$ reflections (triangles), and from the position of the $(-1 + \tau, 0, 7)$ and $(-\tau, 0, 8)$ magnetic reflections (circles). (c) The specific heat shows a clear λ -shaped maximum at the Néel transition. There is no signature of the lock-in transition.

For both samples, the directly measured lattice parameter is in good agreement with the one calculated from the position of the magnetic reflections and with our earlier experiments^{17,19,20,25}. We estimate the relative systematic errors to be below 1×10^{-3} , as indicated in Figs. 3 and 4. Clearly, these are systematic errors – the noise level is at least a factor of 10 smaller.

The importance of using this procedure is underlined by the discrepancy between our value and that given by Choi et al.¹². The latter, $\tau_{\text{Choi}} = 0.548$, can be reproduced from our raw data by simply dividing the low temperature Q -value of the $(2 + \tau, 0, 0)$ reflection, $Q = 4.5823 \text{ \AA}^{-1}$ by the reciprocal lattice parameter at $T = 6.1$ K, $\frac{2\pi}{a} = \frac{1}{2} \cdot Q(2, 0, 0) = \frac{1}{2} \cdot 3.5988 \text{ \AA}^{-1} = 1.7994 \text{ \AA}^{-1}$. Using the high temperature value of $Q(2, 0, 0)$ corresponds to taking the average of the Q -values of the $(2, 0, 0)$ and $(0, 2, 0)$ peaks. We obtain $Q/\frac{2\pi}{a} = 2.547 \approx 2 + \tau_{\text{Choi}}$.

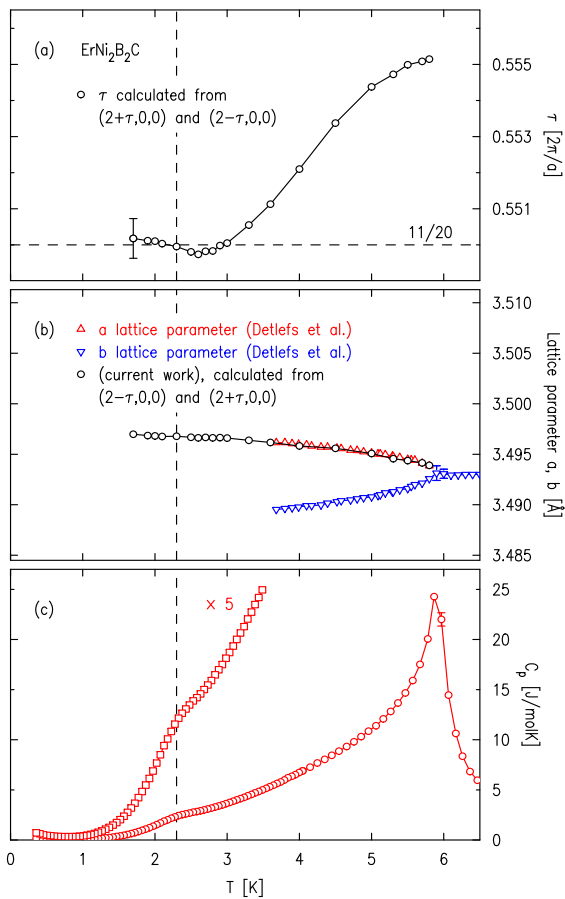


FIG. 4: (a) Around 3 K, the modulation wave vector, τ , of ErNi₂B₂C locks in to the commensurate value of 11/20, indicated by the dashed line. (b) Basal plane lattice parameters, a and b , taken from Ref. 16 (triangles), and from the position of the $(2 + \tau, 0, 0)$ and $(2 - \tau, 0, 0)$ magnetic reflections (circles). (c) In addition to the λ -shaped maximum at the Néel transition, a broad anomaly is observed near the WFM transition.

In both compounds the variation of τ vs. temperature flattens out dramatically as T_{WFM} is approached; within the error cited above their modulation wave vectors agree with the commensurate values indicated by the dashed lines in Figs. 3 and 4. Their absolute values, $\tau_{\text{Er}} = 11/20$, and $\tau_{\text{Tb}} = 6/11$, probably differ because of small difference in the lattice parameters and electronic structures, resulting in different spacings between the nested parts of the Fermi surfaces.

However, there is no sign of a discontinuous change of the modulation at the proposed WFM transition. On the contrary, it appears as if the modulation wave vector was changing continuously, and as if it was not constant, i.e. not locked to a commensurate value, below T_{WFM} . This behavior is confirmed by the neutron data^{12,26}.

Our results are consistent with a second order lock-in transition to the commensurate values given above⁹. In this scenario, the magnetic structure is composed of com-

mensurate blocks separated by domain walls often called “discommensurations”⁹. Across these domain walls the phase of the spin density wave shifts by a defined value, in a way similar to the “spin slip” structures observed in Ho²⁷. The modulation wave vector τ of the structure is obtained from the Fourier transform over several blocks, including the domain walls. The discrepancy between the actual τ and the commensurate value is then proportional to the average phase shift per unit length along the modulation wave vector, i.e. the density of domain walls. When the temperature of the system is varied the domain walls shift until in the limit $T \rightarrow 0$ the distance between them becomes infinite and the wave vector truly commensurate. For ErNi₂B₂C and TbNi₂B₂C, this theory has to be modified to take into account domain wall pinning which is expected to be significant because of the large magneto-elastic strain induced by the orthorhombic distortion associated with the AFM phase transition^{16,17,18}.

The net ferromagnetic moment per formula unit resulting from the above commensurate structures would be $2/N$ of the saturation moment, i.e., $1/10 \mu_{\text{Er}}$ and $2/11 \mu_{\text{Tb}}$, respectively. These numbers have to be compared to the measured fractions (at $T = 2$ K), $0.33 \mu_{\text{B}}/7.8 \mu_{\text{B}} \approx 1/24$ for ErNi₂B₂C³, and $0.55 \mu_{\text{B}}/9.5 \mu_{\text{B}} \approx 1/17$ for TbNi₂B₂C⁶. That the observed WFM moment is significantly smaller than the predicted value might indicate that the saturated, completely ordered state was not reached at the measurement temperature, or that only a finite volume fraction of the sample undergoes the WFM transition. Furthermore, in ErNi₂B₂C the observed magnetization is lowered by the diamagnetism of the superconducting state. Note also that $\tau_{\text{Er}} = 11/20$ does not have the form $N/M\vec{G}$ with N even and M odd, so that the lock-in does not necessarily

induce weak ferromagnetism⁹.

Finally, we note that the specific heat of ErNi₂B₂C exhibits a broad anomaly near the WFM transition (Fig. 4(c)), whereas the specific heat of TbNi₂B₂C (Fig. 3(c)) shows no indication of the WFM transition. This might be related to the different form of the commensurate value, odd/even vs. even/odd, for the Er and Tb compound, respectively⁹.

In summary, we have performed high resolution magnetic x-ray diffraction measurements to study the AFM host structures of ErNi₂B₂C and TbNi₂B₂C close to the weak ferromagnetic transition at T_{WFM} . We determined the modulation wave vector τ with high precision, taking into consideration the magneto-elastic distortion associated with the antiferromagnetic order. In both materials above T_{WFM} τ varies strongly with temperature, whereas below T_{WFM} the variations are much smaller, but still finite and observable. Across the whole temperature range the variations are continuous, so that first order transitions can be excluded. Our observations are consistent with a second order lock-in transition in the presence of discommensurations⁹.

Acknowledgments

The authors are grateful to A. I. Goldman, H. Furukawa-Kawano, P. L. Gammel, and M. B. Walker for stimulating discussions. We also wish to thank the ESRF and the beamline staff of ID10C for assistance with the experiments. Ames Laboratory is operated for the U. S. Department of Energy by Iowa State University under Contract No. W-7405-Eng-82. This work was supported by the Director for Energy Research, Office of Basic Sciences.

* Electronic address: detlefs@esrf.fr

† Current address: Electron Spin Science Center, Department of Physics, Pohang University of Science & Technology, Pohang, 790-784, South Korea.

¹ K.-H. Müller and V. Narozhnyi, eds., *Rare Earth Transition Metal Borocarbides (Nitrides): Superconducting, Magnetic and Normal State Properties* (Kluwer Academic Publishers, Dordrecht, 2001).

² K.-H. Müller and V. N. Narozhnyi, Rep. Prog. Phys. **64**, 943 (2001).

³ P. C. Canfield, S. L. Bud’ko, and B. K. Cho, Physica C **262**, 249 (1996).

⁴ H. Kawano, H. Takeya, H. Yoshizawa, and K. Kadowaki, J. Phys. Chem. Solids **60**, 1053 (1999).

⁵ P. L. Gammel, B. Barber, D. Lopez, A. P. Ramirez, D. J. Bishop, S. L. Bud’ko, and P. C. Canfield, Phys. Rev. Lett. **84**, 2497 (2000).

⁶ B. K. Cho, P. C. Canfield, and D. C. Johnston, Phys. Rev. B **53**, 8499 (1996).

⁷ P. Dervenagas, J. Zarestky, C. Stassis, A. I. Goldman, P. C. Canfield, and B. K. Cho, Phys. Rev. B **53**, 8506 (1996).

⁸ C. Song, J. C. Lang, C. Detlefs, A. Létoublon, W. Good,

J. Kim, D. Wermeille, S. L. Bud’ko, P. C. Canfield, and A. I. Goldman, Phys. Rev. B **64**, R020403 (2001).

⁹ M. B. Walker and C. Detlefs, Phys. Rev. B **67**, 132407 (2003).

¹⁰ S. K. Sinha, J. W. Lynn, T. E. Grigereit, Z. Hossain, L. C. Gupta, R. Nagarajan, and C. Godart, Phys. Rev. B **51**, 681 (1995).

¹¹ J. Zarestky, C. Stassis, A. I. Goldman, P. C. Canfield, P. Dervenagas, B. K. Cho, and D. C. Johnston, Phys. Rev. B **51**, 678 (1995).

¹² S.-M. Choi, J. W. Lynn, D. Lopez, P. L. Gammel, P. C. Canfield, and S. L. Bud’ko, Phys. Rev. Lett. **87**, 107001 (2001).

¹³ H. Kawano-Furukawa, H. Takeshita, M. Ochiai, T. Nagata, H. Yoshizawa, N. Furukawa, H. Takeya, and K. Kadowaki, Phys. Rev. B **65**, R180508 (2002).

¹⁴ D. R. Sánchez, M. A. C. de Melo, M. B. Fontes, S. L. Bud’ko, E. Baggio-Saitovitch, M. Hillberg, W. Wagener, H.-H. Klaus, G. H. Walf, and F. J. Litterst, Phys. Rev. B **57**, 10268 (1998).

¹⁵ J. Jensen, Phys. Rev. B **65**, R140514 (2002).

¹⁶ C. Detlefs, A. H. M. Z. Islam, T. Gu, A. I. Goldman,

- C. Stassis, P. C. Canfield, J. P. Hill, and T. Vogt, *Phys. Rev. B* **56**, 7843 (1997).
- ¹⁷ C. Song, Z. Islam, L. Lottermoser, A. I. Goldman, P. C. Canfield, and C. Detlefs, *Phys. Rev. B* **60**, 6223 (1999).
- ¹⁸ A. Kreyssig, A. Schneidewind, M. Loewenhaupt, C. Ritter, J. Freudenberger, G. Fuchs, and K.-H. Müller, in¹, p. 181.
- ¹⁹ C. Detlefs, D. L. Abernathy, G. Grübel, and P. C. Canfield, *Europhys. Lett.* **47**, 352 (1999).
- ²⁰ C. Song, D. Wermeille, A. I. Goldman, P. C. Canfield, J. Y. Rhee, and B. N. Harmon, *Phys. Rev. B* **63**, 104507 (2001).
- ²¹ D. Gibbs, D. R. Harshman, E. D. Isaacs, D. B. McWhan, D. Mills, and C. Vettier, *Phys. Rev. Lett.* **61**, 1241 (1988).
- ²² J. P. Hannon, G. T. Trammell, M. Blume, and D. Gibbs, *Phys. Rev. Lett.* **61**, 1245 (1988).
- ²³ P. C. Canfield, B. K. Cho, D. C. Johnston, D. K. Finnemore, and M. F. Hundley, *Physica C* **230**, 397 (1994).
- ²⁴ B. K. Cho, P. C. Canfield, L. L. Miller, D. C. Johnston, W. P. Beyermann, and A. Yatskar, *Phys. Rev. B* **52**, 3684 (1995).
- ²⁵ C. Detlefs, A. H. M. Z. Islam, A. I. Goldman, C. Stassis, P. C. Canfield, J. P. Hill, and D. Gibbs, *Phys. Rev. B* **55**, R680 (1997).
- ²⁶ A. Kreyssig, A. Dreyhaupt, K. Krug, R. Schedler, C. Ritter, E. Ressouche, P. Burlet, B. Grenier, K. Prokeš, K. Winzer, et al., *J. Low Temp. Phys.* **131**, 1129 (2003).
- ²⁷ D. Gibbs, D. E. Moncton, K. L. D'Amico, J. Bohr, and B. H. Grier, *Phys. Rev. Lett.* **55**, 234 (1985).
- ²⁸ This cryostat is a prototype of a system now commercially available from A.S. Scientific Products Ltd, Abingdon, UK.